Influence of Elastic Buffer on Rotor Drop Dynamic Response

Zhu Yili[1,a], Xu Longxiang[1,b]
[1]College of Mechanical and Electrical Engineering, Nanjing University of Aeronautics and Astronautics, Nanjing, 210016, PRC
[a]nuaazyl@nuaa.edu.cn, [b]fqp@nuaa.edu.cn

Abstract: In an active magnetic bearing (AMB) system, the rolling-element catcher bearings (CBs) are indispensable to protect the magnetic bearing rotor and stator. This paper introduces a new structure with elastic buffers located on the rotor. And numerical analysis for a rotor drop on CBs using detailed CB model on the basis of Hertz contact theory are presented. The backward whirl of the rotor, which may lead to the destructive damage of the machinery, has been analytically predicted when the system without elastic buffers. The displacements of the sleeve and rotor and also the contact force between the sleeve and the inner-race of the back-up bearing have been computed for various buffer stiffness and damping parameters. Furthermore, elastic buffer design guides based on the simulation results are presented.

Keywords: Rotor Drop, Elastic Buffer, Catcher Bearings, Active Magnetic Bearings

Introduction

Active magnetic bearing (AMBs) have many advantages over conventional mechanical bearings. In addition to supporting the high-speed rotor without any mechanical friction and lubrication, they enable rotor position and induced vibration to be monitored and controlled by adjusting support stiffness and damping. However, the CBs are necessary to protect the AMBs assembly from direct contact with the rotor. They prevent damages during the maintenance and destruction of the system after a possible AMBs failure.

Kirk et al. [1-2] studied the effect of the support stiffness and damping by evaluation of forced response for numerous rotor-support system parameters and showed an optimum damping. Swanson et al. [3] provided the test results for 38 rotor drops with varying rotor speed, unbalance amplitude and location for the 5 CB configurations. Chen et al. [4] proposed the zero clearance auxiliary bearing and presented its performance over conventional CBs. Xie and Flowers [5] numerically investigated the steady-stator behavior of a rotor on CB studied the effects of various parametric configurations: rotor imbalance, support stiffness and damping. Cole et al. [6] developed a deep groove CB model with the elastic deformation of the inner race, which was modeled as a series of flexible beams and studied parametric effects of impact force, bearing width and inner race speed on ball load distributions. However, a rotor drop simulation was not conducted. Wang and Noah [7] analyzed the steady-state response of a rigid rotor in a positive clearance bush using the fixed-point algorithm and predicted a chaotic whirling of the rotor depending on excitation frequency.

However, most of those researches focused on the CBs support stiffness and damping. For it is hard to modify the bearing stiffness and damping to satisfy the optimum simulation results, a new type rotor with elastic buffer is proposed in this paper. A detailed ball bearing model using Hertz contact theory is utilized to gain the real-time support stiffness. The orbit of the rotor in the CBs after the rotor drop and the forces act on the rotor and CBs are obtained through numerical integration of those motion equations. Then the optimum stiffness and damping for the elastic buffer can be determined.

Equations of the studied model

Rotor assembly supported by the magnetic bearings. Figure 1 presents a rotor assembly, AMBs and CBs model considered in this project. The CB is a rolling-element bearing located at the outer-bound of the AMB. Being rigidly assembled on the stator, the CBs are not active during the normal operation of the AMBs. The rotor assembly is composed of a rotor mass with an eccentricity e_r, sleeve masses, and a massless elastic buffer. The symmetric rotor is supported only by the supporting stiffness K_{mb} and the supporting damping C_{mb} when the AMBs are active. Then the equations of motion of the rotor assembly during the normal operation can be written as:

$$\begin{bmatrix} m_r & 0 & 0 & 0 \\ 0 & m_r & 0 & 0 \\ 0 & 0 & m_s & 0 \\ 0 & 0 & 0 & m_s \end{bmatrix} \begin{bmatrix} \ddot{X}_r \\ \ddot{Y}_r \\ \ddot{X}_s \\ \ddot{Y}_s \end{bmatrix} + \begin{bmatrix} C_{mb}+C_f & 0 & -C_f & 0 \\ 0 & C_{mb}+C_f & 0 & -C_f \\ -C_f & 0 & C_f & 0 \\ 0 & -C_f & 0 & C_f \end{bmatrix} \begin{bmatrix} \dot{X}_r \\ \dot{Y}_r \\ \dot{X}_s \\ \dot{Y}_s \end{bmatrix} + \begin{bmatrix} K_{mb}+K_f & 0 & -K_f & 0 \\ 0 & K_{mb}+K_f & 0 & -K_f \\ -K_f & 0 & K_f & 0 \\ 0 & -K_f & 0 & K_f \end{bmatrix} \begin{bmatrix} X_r \\ Y_r \\ X_s \\ Y_s \end{bmatrix} = \begin{bmatrix} m_r e_r^2 \cos(\omega_r t) + m_r g \\ m_r e_r^2 \sin(\omega_r t) \\ m_s g \\ 0 \end{bmatrix} \quad (1)$$

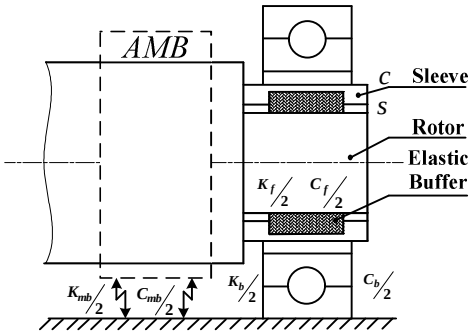

Fig.1 System simplified model

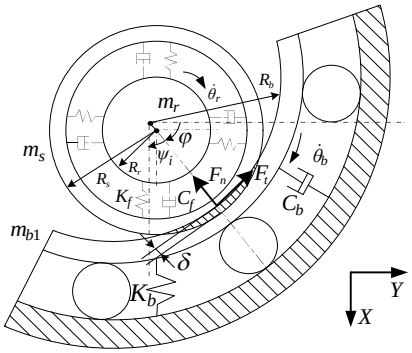

Fig. 2 AMB rotor drop model

Rotor Drop. The rotor drops on the CBs after the AMBs fail. Figure 1 also shows the AMB rotor model after the rotor drop. The elastic buffer is located between the rotor and sleeve to cushion the following series of impact forces. The contact between rotor and sleeve will happen to prevent large displacement of the rotor might leads to the damages of AMBs when the deformation of the elastic buffer is lager than the clearance *s*.

-------Nomenclature----------

$C_{b,mb,f}$	=	support damping of CB, AMB, elastic buffer	f_l	=	Factor depending on CB design and relative load
F_l	=	Force depending on applied CB loads	f_0	=	Factor depending on CB type and lubrication method
F_{nr}	=	contact normal force between rotor and sleeve	g	=	acceleration of gravity
$F_{n,t}$	=	Contact normal, frictional force between inner race and sleeve	$m_{b,r,s}$	=	mass of CB inner race, rotor, sleeve
$J_{r.b}$	=	moment of inertial of rotor assembly, CB inner race	n	=	Inner race angular velocity in r.p.m
K_c	=	Contact stiffness	s	=	Radial clearance between rotor and sleeve
$K_{bx,by}$	=	CB real time stiffness in x-direction, y-direction	t	=	time
$K_{mb,f}$	=	support stiffness of AMB, elastic buffer	ω_r	=	Rotor angular velocity
K_n	=	total contact stiffness between ball and races	ς	=	contact angle of the rotor in sleeve

$R_{b,t}$	=	Radious of innr race, sleeve	ζ_i	=	elastic deformation of each ball
T_b	=	Friction drag torque of CB	γ	=	Bearing radial internal clearance
$X_{b,r,s}$	=	x-direction displacement of CB inner race, rotor, sleeve	δ	=	Contact penetration depth between sleeve and inner race
$Y_{b,r,s}$	=	y-direction displacement of CB inner race, rotor, sleeve	δ_r	=	Contact penetration depth between rotor and sleeve
Z	=	Number of CB balls	μ_d	=	Dynamic sliding friction coefficient
α	=	Contact parameter	ν_0	=	Lubricant kinematic viscosity
c	=	Radial clearance between the sleeve and inner race of CB	φ	=	Angular location of the sleeve in CB
d_m	=	Pitch diameter of CB	ψ_i	=	The *i*th ball position angle
e_r	=	rotor eccentricity	θ_b	=	Angular displacement of inner race

When the sleeve comes into contact with the inner race of the CB, the contact force F_n is induced due to the deformation δ. Meanwhile, coulomb friction forces are acting between the sleeve and inner race of CB, and between the inner race and outer race of the bearing. The driving torque is supposed to be cut off once the AMBs fail. Therefore, the rotor rotating speed is no longer constant. What is more, both support forces of AMBs of the two sides are assumed to close down immediately when a fault situation occurs. Accordingly, it is assumed in this study that the collapsing magnetic force has no effect on the dynamic behavior of the rotor during the drop-down. So the equations of the rotor assembly can be written as:

$$\begin{bmatrix} m_r & 0 & 0 & 0 & 0 \\ 0 & m_r & 0 & 0 & 0 \\ 0 & 0 & m_s & 0 & 0 \\ 0 & 0 & 0 & m_s & 0 \\ 0 & 0 & 0 & 0 & J_r \end{bmatrix} \begin{bmatrix} \ddot{X}_r \\ \ddot{Y}_r \\ \ddot{X}_s \\ \ddot{Y}_s \\ \ddot{\theta}_r \end{bmatrix} + \begin{bmatrix} C_f & 0 & -C_f & 0 & 0 \\ 0 & C_f & 0 & -C_f & 0 \\ -C_f & 0 & C_f & 0 & 0 \\ 0 & -C_f & 0 & C_f & 0 \\ 0 & 0 & 0 & 0 & 0 \end{bmatrix} \begin{bmatrix} \dot{X}_r \\ \dot{Y}_r \\ \dot{X}_s \\ \dot{Y}_s \\ \dot{\theta}_r \end{bmatrix} + \begin{bmatrix} K_f & 0 & -K_f & 0 & 0 \\ 0 & K_f & 0 & -K_f & 0 \\ -K_f & 0 & K_f & 0 & 0 \\ 0 & -K_f & 0 & K_f & 0 \\ 0 & 0 & 0 & 0 & 0 \end{bmatrix} \begin{bmatrix} X_r \\ Y_r \\ X_s \\ Y_s \\ \theta_r \end{bmatrix} = F_r \tag{2}$$

Where

$$F_r = \begin{bmatrix} m_r e_r \left(\dot{\theta}_r^2 \cos\theta_r - \ddot{\theta}_r \sin\theta_r \right) + m_r g - F_{nr} \sin\varsigma \\ m_r e_r \left(\dot{\theta}_r^2 \sin\theta_r - \ddot{\theta}_r \cos\theta_r \right) - F_{nr} \cos\varsigma \\ -F_n \sin\varphi - F_t \cos\varphi + m_t g + F_{nr} \sin\varsigma \\ -F_n \cos\varphi + F_t \sin\varphi + F_{nr} \cos\varsigma \\ -F_t R_s \end{bmatrix} \tag{3}$$

As the outer race of CB is rigidly attached to the stator, the governing equations of motion for the inner race are shown as

$$\begin{bmatrix} m_b & 0 & 0 \\ 0 & m_b & 0 \\ 0 & 0 & J_b \end{bmatrix} \begin{bmatrix} \ddot{X}_b \\ \ddot{Y}_b \\ \ddot{\theta}_b \end{bmatrix} + \begin{bmatrix} C_b & 0 & 0 \\ 0 & C_b & 0 \\ 0 & 0 & 0 \end{bmatrix} \begin{bmatrix} \dot{X}_b \\ \dot{Y}_b \\ \dot{\theta}_b \end{bmatrix} + \begin{bmatrix} K_{bx} & 0 & 0 \\ 0 & K_{by} & 0 \\ 0 & 0 & 0 \end{bmatrix} \begin{bmatrix} X_b \\ Y_b \\ \theta_b \end{bmatrix} = \begin{bmatrix} F_n \sin\varphi + F_t \cos\varphi \\ F_n \cos\varphi - F_t \sin\varphi \\ F_t R_b - T_b \end{bmatrix} \tag{4}$$

The friction drag torque T_b acting on the CB is the sum of two parts. The first part T_l is due to applied loads and can be determined from an empirical evaluation by Palmgren [8].

$$T_l = 2 \times f_l F_l d_m \tag{5}$$

The second part is the viscous friction torque.

$$\begin{cases} T_v = 2\times10^{-7} f_o \left(\nu_o n\right)^{2/3} d_m^3, & \nu_o n \geq 2000 \\ T_v = 320\times10^{-7} f_o d_m^3, & \nu_o n \leq 2000 \end{cases} \tag{6}$$

Figure 2 shows the rotor drop and CB models. In order to calculate conveniently, the nonlinear characteristics caused by different ball positions are ignored. The ball center line is assumed to be just coincident with the direction of the each contact force. Deep groove ball bearing is utilized as CB in this paper, and the real-time bearing support stiffness is determined after computing the stress of each ball using Hertz theory.

The CB support stiffness in the *x* and *y* direction ignoring cross-stiffness can be expressed as:

$$\begin{bmatrix} K_{bx} \\ K_{by} \end{bmatrix} = 2\times\frac{3}{2} K_n \sum_{i=1}^{Z} \left(\zeta_i\right)_+^{1/2} \begin{bmatrix} \sin^2\left(\psi_i+\varphi\right) \\ \cos^2\left(\psi_i+\varphi\right) \end{bmatrix} \tag{7}$$

The contact stiffness K_n is determined based on CB material and geometry. The "+" denotes that only positive ζ_i are included to calculate the bearing support stiffness.

$$\zeta_i = X_{b1}\sin\left(\psi_i+\varphi\right) + Y_{b1}\cos\left(\psi_i+\varphi\right) - \gamma \tag{8}$$

$$\psi_i = \frac{2\pi}{Z}\left(i-1\right), \quad i = 1,2,\cdots,Z \tag{9}$$

Normal forces at the contact points. The contact between the sleeve and the inner race can be modeled using a nonlinear circle-in-circle contact as depicted in Fig. 2. The contact normal force which is a function of the contact penetration and the penetration velocity can be written as follows:

$$F_n = \begin{cases} K_c\delta^{10/9}\left(1+\frac{3}{2}\alpha\dot{\delta}\right), & \delta > 0 \\ 0, & \delta \leq 0 \end{cases} \tag{10}$$

Where

$$\delta = \sqrt{\left(X_s - X_b\right)^2 + \left(Y_s - Y_b\right)^2} - c \tag{11}$$

Similarly, the contact force between the rotor and sleeve can also be determined adopting the circle-in-circle model. Assuming they have the same contact damping and stiffness:

$$F_{nr} = \begin{cases} K_c\delta_r^{10/9}\left(1+\frac{3}{2}\alpha\dot{\delta}_r\right), & \delta_r > 0 \\ 0, & \delta_r \leq 0 \end{cases} \tag{12}$$

Where

$$\delta_r = \sqrt{\left(X_r - X_s\right)^2 + \left(Y_r - Y_s\right)^2} - s \tag{13}$$

Friction force at the contact point. The friction force is proportional to the contact normal force as long as slipping exists at the contact point.

$$F_t = \mu_d F_n \tag{14}$$

However, the friction force changes once there is no slip at the contact point. So a rolling condition is applied to the model to calculate the friction force when the tangential velocity of the inner race reaches that of the shaft at the contact point.

For rolling condition:

$$\dot{\theta}_r R_s = \dot{\theta}_b R_b \tag{15}$$

By arranging equations (2), (4) and (15), the friction force becomes

$$F_t = \frac{J_r R_b T_b}{J_r R_b^2 + J_b R_s^2} \tag{16}$$

If the circumferential speeds at the contact point become equal, the sleeve and the inner race will keep contacting without a slip as long as the friction force does not exceed the maximum static frictional force ($\mu_s F_n$). Where μs is the coefficient of static sliding friction between the sleeve and inner race of CB.

Results analysis

Rotor drop simulations are conducted to illustrate implementation of the model capabilities and to identify a good elastic buffer design. The studied model dimension and material characteristics are shown in Table 1. Numerical integration of the equations of motions for the system model listed above is performed using the forth-order Runge-Kutta integration algorithm with a variable time step. Firstly, the equation (1) for the rotor assembly motion when the AMBs are active is solved. And the magnetic bearings are assumed to be cut off when the rotor geometric center crosses the X-axis at the lower point after the motion goes into steady-state circular synchronous precession. Then the motion parameters of this point are used as the initial condition to solve the rotor drop equation (3).

Table 1
Parameters of the studied model

Dimension and property	Specification
CB width, B (mm)	9
CB damping, C_b (N-s/m)	200
Buffer damping, C_f (N-s/m)	1500
AMB damping, C_{mb} (N-s/m)	15E+3
Air gap between sleeve and CB, c (mm)	0.125
Inner diameter, d_i (mm)	25
Outer diameter, d_e (mm)	42
Pitch diameter, d_m (mm)	33.5
Modulus of elasticity, E (MPa)	207000
Plolar moment of inertia of CB inner race, J_b (kg m^2)	1E-4
Plolar moment of inertia of rotor assembly, J_r (kg m^2)	0.005
Stiffness of contact, K_c (N/m)	5E+8
Stiffness of AMB, K_{mb} (N/m)	2E+6
Mass of CB inner race, m_b (kg)	0.02
Mass of rotor, m_r (kg)	5
Mass of sleeve, m_s (kg)	0.5
Radial clearance between rotor and sleeve, s (mm)	0.2
Inner and outer race conformity	0.52

Contact parameter, α	0.08
Diametric clearance, γ (μm)	5
Dynamic sliding friction coefficient, μ_d	0.2
Static sliding friction coefficient, μ_s	0.3
Number of balls, z	12
Poisson's ratio, v	0. 3
Viscosity of lubricant, υ_0 (cSt)	25

Figures 3(a)-(b) show the maximum contact normal forces between the sleeve and inner race of CBs for various buffer parameters. The maximum contact forces during rotor drop processes in very light buffer damping cases are extremely large, and some of them have exceeded the maximum load the CB can withstand. When the buffer parameters are K_f between 7E+5-5E+6 N/m and C_f between 2000-8000 N-s/m, the contact normal forces are relatively small, and the CBs won't be damaged. The sleeve and rotor will collide in small buffer stiffness and damping cases as shown in Fig.4.

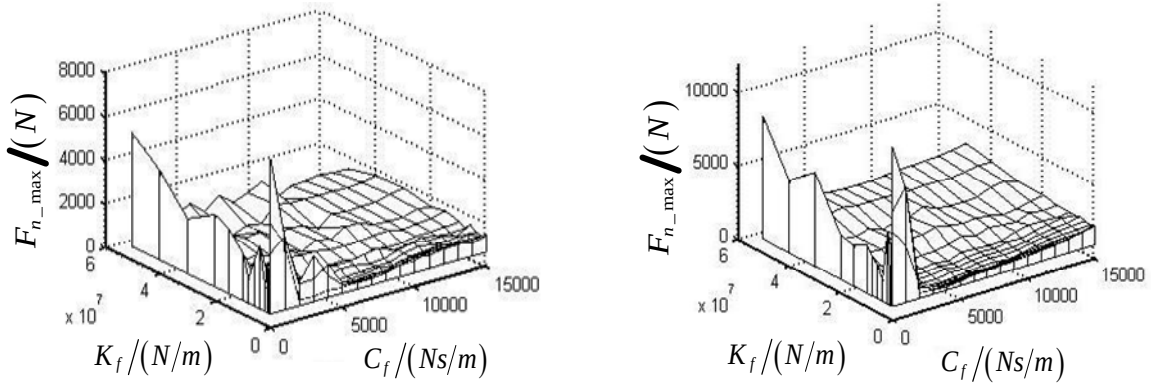

(a) (b)

Fig. 3 maximum contact force maps between sleeve and inner race for various buffer parameters (a) rotor initial speed 20000. rpm (b) rotor initial speed 30000. rpm

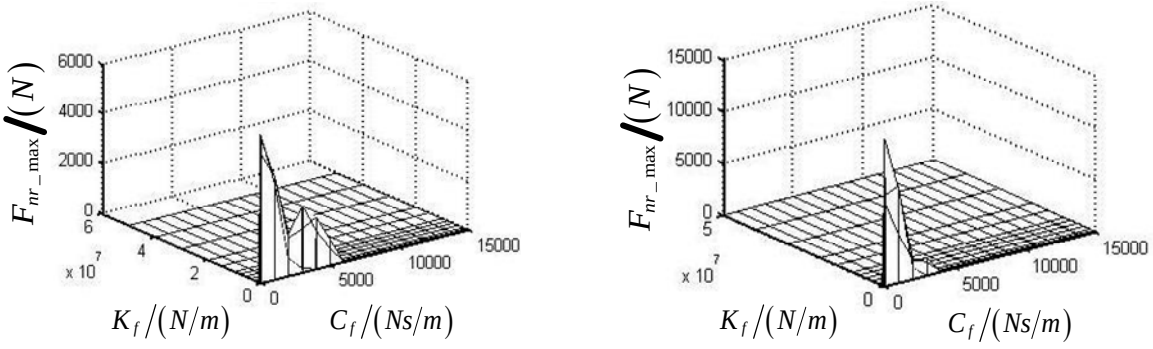

(a) (b)

Fig. 4 contact force maps between sleeve and rotor for various buffer parameters (a) rotor initial speed 20000 rpm (b) rotor initial speed 30000 rpm

Figures 5 (a)-(b) show the orbits of the rotor and sleeve of the rotor assembly model for various buffer parameters. The inner circle represents the clearance circle of the CB. The sleeve often exceeds the clearance circle because of the deformation of the CB as well as the contact point. The small circles near the origin are the steady-state orbits before AMB failure. The rotor displacements are relatively larger and sometimes even exceed the AMB circle for

the deformation of the fixed buffer. In the light stiffness and damping case, the sleeve keeps bouncing in the inner race after rotor drop. While the sleeve begins to rock back and forth in the bottom of the inner race after a few times of bounces when appropriate stiffness and damping are adopted as shown in fig 5(b).

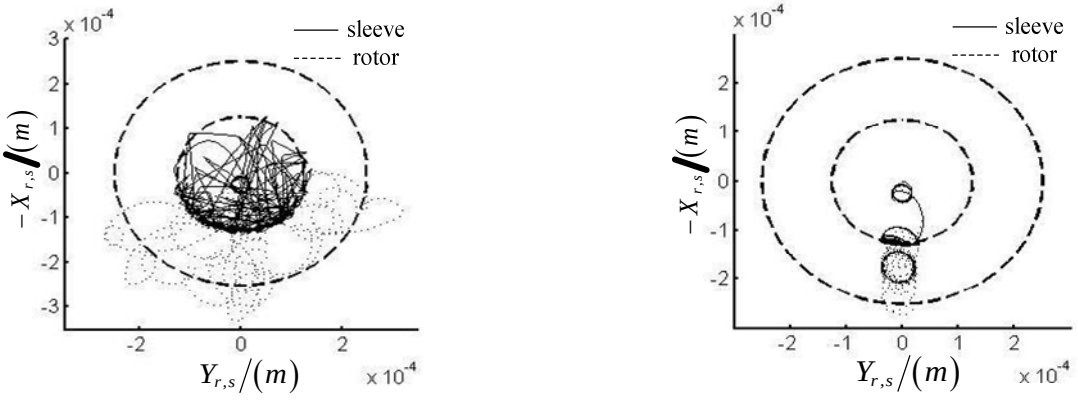

(a) (b)

Fig. 5 the orbits of the rotor and sleeve after the rotor drop t = 0-0.1s for the initial rotor speed 20000 rpm. (a) K_f = 5E+4. N/m, C_f = 0. N-s/m (b) K_f = 1E+6. N/m, C_f = 2000. N-s/m

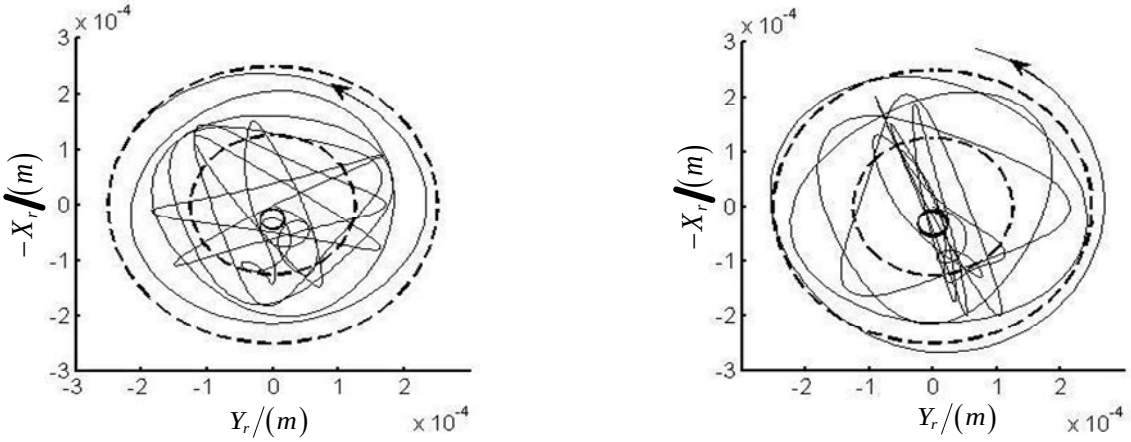

(a) (b)

Fig. 6 the orbit of rotor after rotor drop t = 0-0.02s without buffer and sleeve (a) rotor initial speed 20000. rpm (b) rotor initial speed 3000. rpm

Figures 6 (a)-(b) show that the backward whirl motion will happen in the rotor system model without elastic buffer. When the AMB system becomes inactive, the rotor drops on the CB and bounces several times on the inner race. And then the rotor begins to rotate all around and finally gets into backward whirl motion. Once the backward whirl occurs, the displacement of the rotor grows larger and larger, which may lead to the contacts between rotor and stator lamination.

Conclusion

This paper introduced a new rotor structure to reduce the damage caused by AMB failure. And the rotor assembly with elastic buffer model is established. Detailed CB model is presented to calculate the real time support stiffness during the rotor drop process. And then the influences

of the elastic buffer stiffness and damping are analyzed to find the parameters that satisfy the design objectives. The conclusions for the model considered in this paper are:

(1) The optimum elastic buffer parameters are K_f between 7E+5-5E+6 N/m and C_f between 2000-8000 N-s/m. In this range the contact normal forces between sleeve and CB inner race are relatively small. And the sleeve and rotor do not collide even the rotor initial speed is extremely high after rotor drop.
(2) Appropriate elastic buffer parameters also help to control the sleeve and rotor from high amplitude vibration after the AMB system does not operate.
(3) The backward whirls happen shortly after the rotor drop on the CB when the new structure is not adopted, which may lead to the destruction of the whole system.
(4) Considering the large displacement of rotor because of the elastic buffer deformation, the air gap between rotor and AMB stator can be increased appropriately to avoid their collision after rotor drop. And the inadequate bearing capacity can be made up through increasing the bearing coil turns.

Acknowledgment

The authors gratefully acknowledge the support of the National Natural Science Foundation of China (Grant No. 50975134).

References

[1] T. Ishii, R.G. Kirk: Journal of Rotating Machinery and Vehicle Dynamics 35 (1991) 191-199.
[2] R.G. Kirk, T. Ishii: Proceedings of MAG'93 Magnetic Bearings, Magnetic Drives, and Dry Gas Seals Conference & Exhibition, Alexandria, VA, USA, 1993, pp. 53-61.
[3] E.E. Swanson, R.G. Kirk, J. Wand: Proceedings of MAG'95 Magnetic Bearings, Magnetic Drive and Dry Gas Seals Conference & Exhibition, Alexandria, VA, USA, 1995, pp. 207-216.
[4] H.M. Chen, J. Walton, H. Heshmat : Proceedings of MAG'97 Industrial Conference and Exhibition on Magnetic Bearings, Alexandria, VA, USA, 1997, pp. 111-119.
[5] H. Xie, G.T. Flowers: American Society of Mechanical Engineers Winter Annual Meeting, Chicago, USA, 1994, pp.1-11.
[6] M.O.T. Cole, P.S. Keogh, C.R. Burrows: Journal of Tribology 124 (2002) 406-413.
[7] X. Wang, S. Noah: Journal of Vibration and Acoustics 120 (1998) 576-606.
[8] T.A. Harris, Rolling Bearing Analysis, 2nd Edition, Wiley-Inter science Publication, New York, 1984